Optimization of Graphene on D-Fiber Saturable Absorbers

Daniel Felipe Londono-Giraldo, Eunezio Antonio Thoroh De Souza, and Hugo Luis Fragnito

***Abstract*—The graphene-light interaction in a waveguide can be optimized through the waveguide design. In the case of nonlinear optical devices, such as saturable absorbers, this optimization requires knowledge of the actual intensity that quantifies the nonlinear interaction with a waveguide mode. In this work we propose parameters that correctly quantify the strength of saturable absorption. We show that the graphene on D-fiber saturable absorber can be characterized through the absorption coefficient and a properly defined saturation power for each mode. We analyze the dependence of the graphene-light interaction on the geometrical parameters, chemical potential, number of graphene layers, and input power. The results show a wide variation of the graphene absorption with the design, which offers potential for polarizers with large polarization extinction ratios and saturable absorbers with low saturation powers. As a function of the number of layers, the interaction is maximized for five layers, and we predict a reverse saturable absorption effect for higher number of layers. The parameters introduced here to quantify the nonlinear graphene-light interaction can be applied to other waveguide structures and other 2D materials.**

***Index Terms*—Graphene, optical fiber devices, optical waveguide components, saturable absorbers.**

I. Introduction

THE integration of graphene and other 2D materials into optical waveguides offers extended interaction lengths versus the one-atom thickness of normal incidence. In turn, this allows to better exploit the optical properties of these materials. Side-polished fibers or D-fibers are especially attractive for all-fiber systems, such as fiber lasers [1]–[4], fiber sensors [5]–[7] and in-line optical switches and modulators [8], [9], since they are easy to fabricate with low insertion loss (< 0.5 dB) [10], [11].

Graphene interacts with light mainly through optical absorption. When graphene is integrated into D-fibers, the absorption can be designed to be highly dependent on the polarization, potentially resulting in broadband, large polarization extinction ratio polarizers [11]–[14]. Additionally, the absorption can be varied electrically to develop optical switches and modulators [8] and lasers with electrically controlled operation regime (continuous wave, Q-switching, or mode-locking) [10], or it can be controlled optically, to produce all-optical switches [9], [15] and saturable absorbers [10], [11], [16]–[20]. In particular, this type of saturable absorber is a very efficient passive mode-locker for fiber lasers, resulting in lasers that emit very short light pulses [11].

The graphene-light interaction in a bare polished fiber is relatively weak [16], [21]. This is due to the low refractive index of air ($n = 1$) above the graphene layer. The interaction can be improved by covering graphene with an over-cladding [16] or with a superstrate [13], [21]. In the case of an over-cladding, the refractive index of the new material is equal to or smaller than the refractive index of the cladding. In this way, the over-cladding can have an arbitrarily large thickness. In [16], the authors show that the graphene-light interaction increases as the over-cladding refractive index approaches the cladding refractive index. Therefore, in this case, an index-matched over-cladding provides the strongest interaction. The interaction can be further improved by using a superstrate with a refractive index slightly larger than the core refractive index. In [13], the authors show that increasing the thickness of a PVB superstrate improves the polarization extinction ratio of the graphene on D-fiber (GDF) device.

So far, reported GDF saturable absorbers were not optimized. The optimization of the GDF as a saturable absorber is difficult, since the actual intensity that drives saturation depends on many parameters. In the literature on the modal analysis of GDFs, the graphene-light interaction is usually evaluated through the mode absorption coefficient [8], [22]. This is sufficient for a polarizer. However, for nonlinear optical devices such as a saturable absorber we need to identify which component of the Poynting vector actually interacts with graphene. The definition of this intensity for an arbitrary mode is not straightforward, especially in the case of TM modes. Furthermore, an appropriate spatial averaging of this intensity along the transverse direction of graphene is necessary to correctly account for the nonlinear interaction. We propose a definition of an effective graphene width, and, accordingly, a mean absorbed intensity, that correctly characterize the nonlinear optical response of the device. These parameters facilitate the optimization of the device as a function of the geometry and number of graphene layers. In the multilayer case, we find that there is an optimum number of layers, and beyond that number we predict a reverse saturable absorption effect.

In this paper, we analyze the graphene-light interaction and how this depends on the cross-section geometry, pointing to configurations that optimize nonlinear optical devices. We analyze

Manuscript received 30 March 2022; revised 10 June 2022; accepted 27 June 2022. Date of publication 4 July 2022; date of current version 16 September 2022. *(Corresponding author: Hugo Luis Fragnito.)*

Daniel Felipe Londono-Giraldo and Eunezio Antonio Thoroh De Souza are with the Mackenzie Presbyterian University, São Paulo 01302-907, Brazil (e-mail: danielf.londono@udea.edu.co; thoroh@mackenzie.br).

Hugo Luis Fragnito is with the Gleb Wataghin Physics Institute, University of Campinas, Campinas 13083-970, Brazil (e-mail: fragnito@unicamp.br).

Color versions of one or more figures in this article are available at https://doi.org/10.1109/JLT.2022.3188216.

Digital Object Identifier 10.1109/JLT.2022.3188216

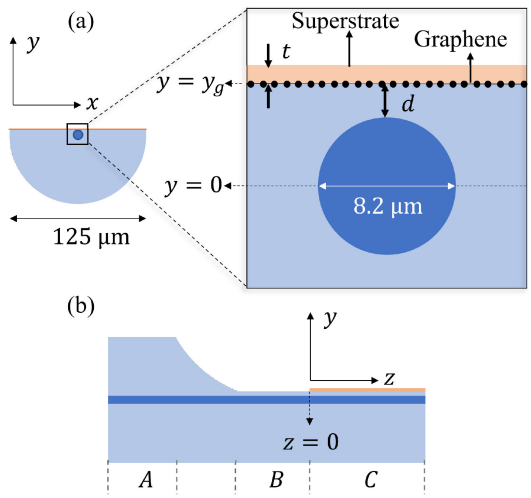

Fig. 1. Schematic diagram of the GDF device. (a) Transverse view of the GDF. The zoomed region illustrates the gap distance d between graphene and the fiber core and the thickness t of the superstrate layer. (b) Longitudinal view of the GDF. Sections A, B, and C correspond to the unpolished fiber, the polished fiber, and the GDF, respectively.

how the GDF depends on the intrinsic parameters of graphene (chemical potential and scattering rate), number of layers, and the power coupling across the interfaces from the input fiber to the GDF. This allows for an accurate modeling of GDF devices, including saturable absorbers and polarizers. To describe GDF saturable absorber we propose a saturation parameter that is compatible with that usually defined for normal incidence. The same approach can be extended to other waveguide geometries and to other 2D materials.

II. Model of the GDF (Graphene on D-Fiber)

The D-fiber considered in this paper (Fig. 1) is obtained by side-polishing a standard single mode fiber, to produce a flat surface at a short distance d from the fiber core. The standard fiber considered has a step index profile with a core diameter of 8.2 μm, 125 μm external clad diameter, and (at a wavelength $\lambda = 1550$ nm) refraction indices of 1.4492 and 1.444 in the core and cladding, respectively. Graphene is directly on top of the polished surface (at $y = y_g$) and covered by a superstrate of thickness t and refraction index $n = 1.490$ at 1550 nm (corresponding to the commonly used polymer polymethyl methacrylate - PMMA).

We solved the eigenmodes of the GDF by using the same simulation methodology as in reference [23], where graphene is considered as an ideal material without thickness, simulated through its optical surface conductivity σ [24], and using boundary conditions. At room temperature, at the wavelengths considered, and at low optical powers, $\sigma \approx e^2/4\hbar = 60.8$ μS, where e is the electron charge and $\hbar$ is the reduced Planck constant. This is valid for graphene at low doping levels, such that the absolute value of the chemical potential ($|\mu|$) is small compared to half the photon energy of the optical field ($hc/2\lambda$). Unless otherwise specified, we consider undoped graphene ($\mu = 0$). The influence of μ is analyzed in Section III-D. The mode solver uses $\sigma = (60.8 - i0.04)$ μS, but the small imaginary part is essentially irrelevant.

The modes of the D-fiber can be of (quasi) TE or TM character, depending on the state of polarization of the input field in the standard fiber. The TE (TM) mode has the electric (magnetic) field mostly parallel to the graphene plane. Rigorously speaking, the electric or magnetic fields of these modes are not purely transverse to the propagation axis z, and in this respect are classified as quasi-TE or quasi-TM.

The strength of the light-graphene interaction is determined by the absorption coefficient α_g and the absorbed intensity by graphene, I_g (defined below). This last is of key relevance for nonlinear optical processes, such as saturable absorption. These parameters depend on the particular optical mode excited by the input field, and are obtained from the mode solver. Nevertheless, it is useful to have analytical expressions to gain insights on how they depend on the mode distribution.

A guided mode is represented by an electric field of the form $\mathbf{E}(x,y)e^{i\beta z - \alpha z/2}$ and identical forms for the magnetic field and the current density with corresponding vectors $\mathbf{H}(x,y)$ and $\mathbf{J}(x,y)$. Here α is the loss coefficient and β, the propagation constant, defines the effective index of the mode through $\beta = 2\pi n_{\text{eff}}/\lambda$. The Poynting vector is represented as $\mathbf{S}(x,y)e^{-\alpha z}$, with

$$\mathbf{S}(x,y) = \frac{1}{2}\text{Re}\left\{\mathbf{E}(x,y) \times \mathbf{H}^*(x,y)\right\}. \tag{1}$$

The power carried by the mode attenuates as $P(z) = P(0)e^{-\alpha z}$ where the launched mode power is given by integrating the z-component of $\mathbf{S}(x,y)$ over the entire xy plane:

$$P(0) = \iint S_z(x,y)dxdy. \tag{2}$$

In this work we assume that the loss coefficient $\alpha = \alpha_g$ is due only to the (ideal) conductivity of graphene. Other spurious losses (α_{sp}) from graphene rugosity and impurities (as well as losses not due to graphene) contribute to the total loss coefficient $\alpha = \alpha_g + \alpha_{sp}$. For simplicity, we do not consider these extra losses in our analysis, but their inclusion is straightforward. If the only lossy material is graphene, then $\mathbf{J}(x,y) = \mathbf{J_s}(x)\delta(y - y_g)$, with the surface current $\mathbf{J_s}(x) = \sigma\mathbf{E}_\parallel(x,y_g)$, where $\mathbf{E}_\parallel(x,y_g) = \hat{\boldsymbol{x}}E_x(x,y_g) + \hat{\boldsymbol{z}}E_z(x,y_g)$ is the electric field parallel to- and on- the plane of graphene. Only the electric field components parallel to the graphene plane contribute to absorption, and in the following we focus on these components.

In this surface conductivity model, the absorbed power per unit area of a given mode is always given by $\frac{1}{2}\sigma'|\mathbf{E}_\parallel(x,y_g)|^2e^{-\alpha_g z}$, where $\sigma' = \text{Re}\{\sigma\}$. Integrating over x we obtain the absorbed power per unit length $-dP/dz = \alpha_g P$, thus

$$\alpha_g = \frac{1}{2P(0)}\int_g \sigma'|\mathbf{E}_\parallel(x,y_g)|^2dx. \tag{3}$$

It is interesting to derive α_g from the Poynting theorem and the boundary conditions: The absorbed power in a segment of graphene of length dz is given by the inward flux of $\mathbf{S}$ through a closed surface tightly enclosing the graphene segment. This flux is not zero since the normal component S_y is discontinuous,

on account for the discontinuity of the magnetic field, $\Delta\mathbf{H}_{\|} = \mathbf{H}(x, y_g^+) - \mathbf{H}(x, y_g^-) = \hat{\boldsymbol{y}} \times \mathbf{J}_{\mathbf{s}}(x)$, as required by the boundary condition for $\mathbf{H}_{\|}$ (H_y and $\mathbf{E}_{\|}$ are continuous). This gives $\Delta S_y = \frac{1}{2}\hat{\boldsymbol{y}} \cdot \mathrm{Re}\{\mathbf{E}_{\|} \times \Delta\mathbf{H}_{\|}^*\} = \frac{1}{2}\sigma'|\mathbf{E}_{\|}|^2$. Thus, the flux per unit length $\int_g \Delta S_y(x)dx = \frac{1}{2}\int_g \sigma'|\mathbf{E}_{\|}(x, y_g)|^2 dx = -dP/dz$, and one arrives again to (3). This deduction shows that there is a component of the Poynting vector normal to the graphene plane, even if, in many cases, the mode in this region has some characteristics of an evanescent field or of a grazing incidence wave. It is S_y, and not S_z, that is relevant to quantify the graphene-light interaction. One can think of $\Delta S_y(x)$ as the sum of the absorbed intensity of waves hitting graphene from both sides, and we are interested in its average over the x dimension.

We define the (x-averaged) absorbed intensity, I_g, as the absorbed power ($-dP$) per unit area $dA = w_{\text{eff}}dz$, where w_{eff} is an effective graphene width:

$$I_g(z) = -\frac{1}{w_{\text{eff}}}\frac{dP}{dz} = \frac{\alpha_g}{w_{\text{eff}}}P(z), \tag{4}$$

where

$$w_{\text{eff}} = \frac{\left(\int_g |\mathbf{E}_{\|}(x, y_g)|^2 dx\right)^2}{\int_g |\mathbf{E}_{\|}(x, y_g)|^4 dx}. \tag{5}$$

These definitions are not unique, and other values for w_{eff} and I_g could be adopted, as along as the product $w_{\text{eff}}I_g = \alpha_g P$. Since we consider that the nonlinearity is exclusively due to graphene, the effective width plays the role of the effective area in nonlinear waveguide optics. For values of d and t that do not perturb severely the mode relative to that of the fiber, w_{eff} given in (5) is approximately equal to the diameter of the fiber core. Note that α_g does not depend on the coupling coefficients, but I_g does depend.

If we take as reference the incident power before the D-fiber (P_0), then the power at the beginning of graphene ($z = 0$) can be expressed as $P(0) = \mathcal{C}_{AB}\mathcal{C}_{BC}P_0$, where $\mathcal{C}_{AB}$ is the power coupling coefficient from the unpolished fiber (A) to the bare polished fiber (B), and $\mathcal{C}_{BC}$ is the power coupling coefficient from the bare polished fiber (B) to the GDF (C) (see Fig. 1). The computed mode of the input standard single mode fiber is the exact HE_{11} mode (but we don't expect any relevant variation if the LP_{01} mode is assumed). We computed these coefficients from the overlap integral between the modes of adjacent sections, a procedure that is appropriate for abrupt transitions. The transition BC is indeed abrupt, but the transition AB may occur gradually (or 'adiabatically') over a certain length, as illustrated in Fig. 1, and in that case $\mathcal{C}_{AB}$ will depend on the details of the polishing procedure. An abrupt transition corresponds to a worst-case scenario, underestimating the actual coupling. A detailed account of how the coupling coefficients depend on d and t is presented in [25].

III. Results

A. D-Fiber Design

We first analyze the strength of the graphene-light interaction as a function of the gap distance. Fig. 2 shows α_g and I_g (at $z = 0$) for each mode and two superstrate thicknesses. As we expected, TE modes are more absorbed than the TM modes. This is because in the TE case the interaction is through their strongest component, E_x, whereas in the TM case the interaction comes through their comparatively weaker E_z component.

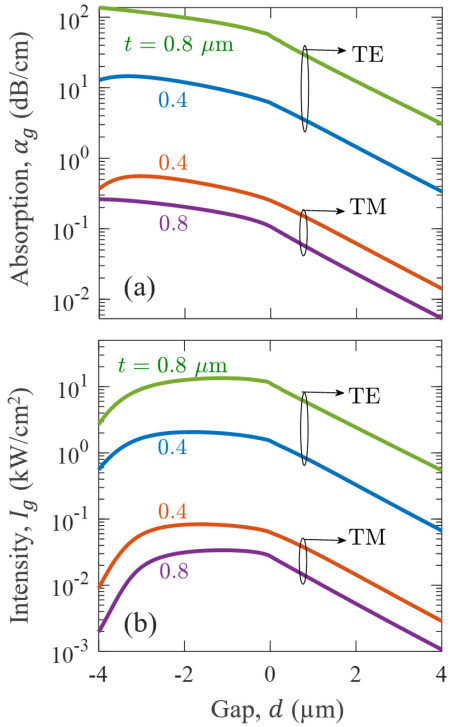

Fig. 2. Graphene-light interaction as a function of the gap distance. Two superstrate thickness are shown for each mode: (a) absorption coefficient; (b) absorbed intensity (at $z = 0$ and for $P_0 = 1$ W).

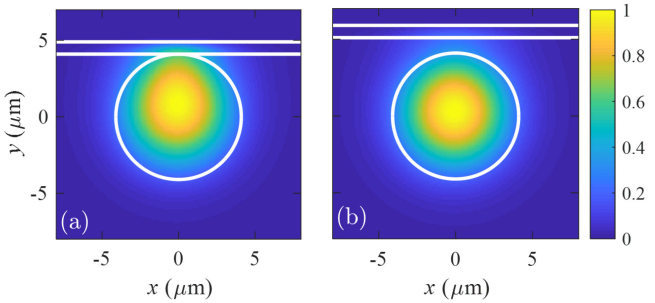

Fig. 3. Normalized $|\mathbf{E}_{\|}(x, y)|^2$ for the TE mode, $t = 0.8$ μm, and (a) $d = 0$, (b) $d = 1$ μm.

For positive gaps, both curves in Fig. 2(a) and (b) are linear in semi-log scales, indicating that the interaction with graphene decays exponentially with increasing gap. This reflects the essentially evanescent nature of the modal fields in the cladding. We illustrate this in Fig. 3 for the TE mode, where we show $|\mathbf{E}_{\|}(x, y)|^2$ for two gap distances ($d = 0$ and $d = 1$ μm) and a fixed $t = 0.8$ μm.

Returning to Fig. 2, the interaction keeps increasing as the gap is reduced, even in the negative gap range, up to certain point (between $d = -2$ μm and $d = -1$ μm for the examples in this

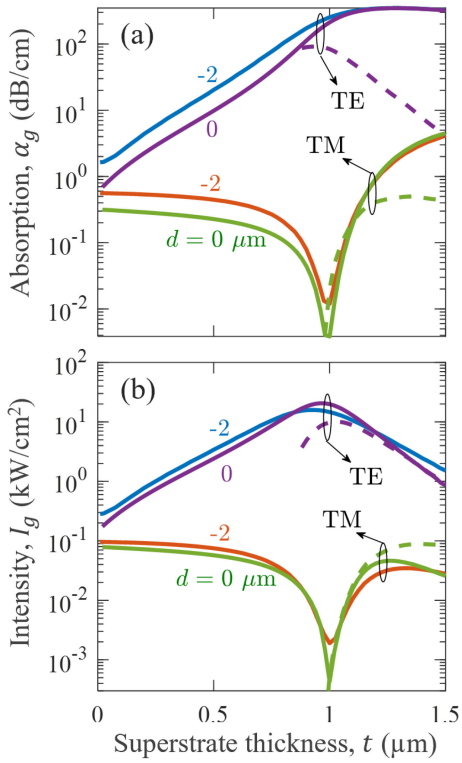

Fig. 4. Graphene-light interaction as a function of the superstrate thickness. Two gap distances are shown for each mode: (a) absorption coefficient; (b) absorbed intensity (at $z = 0$ and for $P_0 = 1$ W).

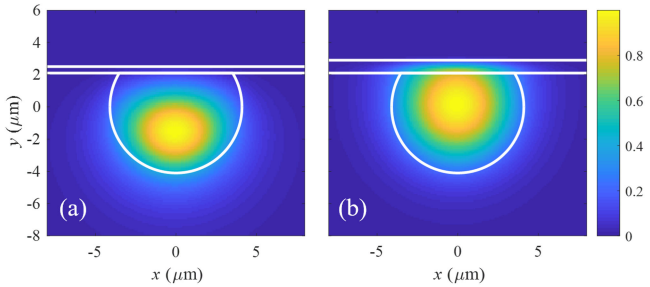

Fig. 5. Normalized $|\mathbf{E}_{\|}(x, y)|^2$ for the TE mode, $d = -2$ μm, and (a) $t = 0.4$ μm, (b) $t = 0.8$ μm.

figure). Reducing the gap further ($d < -2$ μm), the intensity decreases more abruptly (Fig. 2(b)), this is because the coupling (that affects I_g but not α_g) becomes highly inefficient due to the large mismatch between the modes of adjacent sections A and B.

Next, we consider the variation of the superstrate thickness, t. Fig. 4 shows α_g and I_g for each mode and two gap distances. We can see that from $t = 0$ up to $t \approx 1$ μm, the TE and TM modes have opposite trends, that is, the interaction with graphene for increasing t increases for the TE mode, but decreases for the TM mode. In order to understand physically this difference, we analyze first the behaviour of the TE mode, with the help of Fig. 5. This Figure shows $|\mathbf{E}_{\|}(x, y)|^2$ for the TE mode, for a fixed gap $d = -2$ μm and two superstrate thicknesses. In the case of the thinner superstrate ($t = 0.4$ μm), the mode is *repelled* by the lowest refractive index (of air) above the thin superstrate, and therefore concentrates away from the superstrate. In contrast, for the thicker superstrate ($t = 0.8$ μm), the modal field concentrates near the superstrate, which is now thick enough to accommodate a part of the mode.

For the TM mode, $|\mathbf{E}_{\|}(x, y)|^2$ exhibits a completely different behavior, being highly concentrated on the superstrate–air interface. Therefore, as t increases, the peak of this intensity *moves* farther away from the graphene plane, effectively reducing the graphene-light interaction.

As the superstrate thickness increases, high order modes appear, depending on the gap distance. This is because, for large enough d and t, the superstrate acts as a second core. In this situation, there are two TE and two TM guided modes, where the fundamental modes are mostly located in the superstrate (that has the highest refractive index), and the second-order modes are mostly located in the core.

In Fig. 4 for $d = 0$, the second order TE and TM modes appear at $t = 0.88$ μm and $t = 0.98$ μm, respectively. Differently, in the case of $d = -2$ μm, the waveguide only supports the fundamental guided modes. Multimode waveguides are more sensitive to thermal fluctuations that may lead to erratic operation. Additionally, for thick superstrates, $t > 1.2$ μm, the coupling to the fundamental 'superstrate' modes becomes highly inefficient. Hence, we propose the cutoff of the second order mode as a criterium for setting the maximum value of t.

Optimizing a nonlinear optical device implies in maximizing I_g. This parameter includes the effects of minimizing w_{eff}, and maximizing the coupling coefficients and the absorption coefficient. One can see in Figs. 2 and 4 that the intensity I_g is maximized for $d \approx 0$ and $t \approx 1$ μm, but if we limit ourselves to single mode operation, then the maximum is obtained at cutoff of $t = 0.88$ μm. Therefore, a device with $t = 0.8$ μm provides a margin for stable single mode operation and I_g close to the maximum possible value. In the following we shall refer to this design ($d = 0$, $t = 0.8$ μm) as the 'optimized' device. In experiments, the polymer is deposited by spin-coating, resulting in a typical thickness of 300 nm [11]. In comparison, as shown in Fig. 4, our optimized device will produce at least a tenfold increase in the absorbed intensity. For the TE mode of the optimized device, the ratio of the absorbed intensity to the mean incident intensity (in the unpolished fiber) is 0.9%.

B. Number of Graphene Layers

We can extend the framework to model few-layers graphene, in this case the conductivity is scaled by the number of layers (N) in the absence of interlayer interactions. For large N, the validity of the boundary conditions approach employed in this work may be questionable, since the continuity of $\mathbf{E}_{\|}(x, y)$ may not hold. Nevertheless, the analysis is useful to provide insights on how the multilayer device behaves. Ultimately, the analysis is rigorously valid for a hypothetical 2D material having a conductivity $N\sigma$. In Fig. 6 we show α_g as a function of the number of graphene layers ($N = 1 - 20$ layers) for $d = 0$, $t = 0.4$ μm and $t = 0.8$ μm (the GDF is single mode for any N).

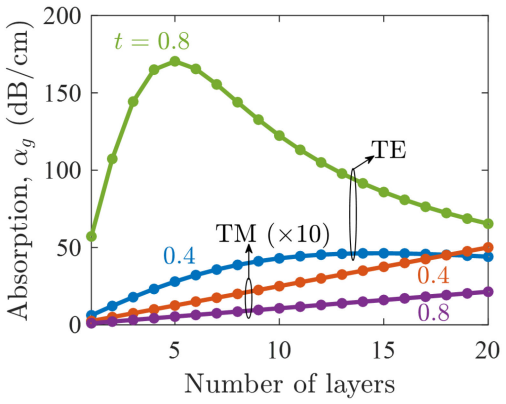

Fig. 6. Absorption coefficient as a function of the number of layers.

The absorption of both TM modes and the TE mode for $t = 0.4\ \mu$m continuously increases in this range, due to the increased conductivity of the graphene plane. Differently, the absorption of the TE mode for $t = 0.8\ \mu$m increases only up to 5 layers, and then decreases. This is because by further increasing the conductivity (thus tending to a perfect conductor where $\sigma = \infty$ and $|\mathbf{E}_{\|}(x, y_g)| = 0$) the mode *moves away* from graphene, reducing the absorption. Therefore, adding more than 5 graphene layers does not further improve the graphene-light interaction in this case. Note that although the conductivity $\sigma_N = N\sigma$, α_g is not proportional to N.

C. Saturable Absorption

Consider now the application of this device as a saturable absorber. We start by noting that since the local intensity depends on x, the saturated conductivity is also a function of x. Solving the modes in this case is a challenging problem, because the mode depends on the conductivity and in turn the conductivity depends on the mode. Because of the attenuation, there is also a z-dependence on saturable conductivity that in principle breaks down the translational invariance. Rigorously, the exponential attenuation of the modes is no longer valid, and the waveguide should be treated as a tapered one, further complicating the simulations. We do not attempt to solve the exact propagation equations, and we limit our analysis of the saturated response of the GDF for $z = 0$, and assuming a constant, x-averaged conductivity. This is equivalent to having a different 2D material with a non-saturable conductivity, an approximation that is better for weak saturation.

Saturable absorbers are often characterized by a saturation parameter $s = I/I_s$, where I is the intensity and I_s is the saturation intensity, such that for $I = I_s$ the absorption coefficient drops to 1/2 of the linear case. For the case of normal incidence, I is the incident intensity, but in our case, we demand a proper definition, since not all the components of the Poynting vector really interact with graphene. In our problem, we can introduce a fictitious (equivalent normal incident) intensity I_{eff} such that the absorbed intensity is $I_g = I_{\text{eff}}\eta_0\sigma'/n_{\text{eff}}$, where $\eta_0 = 377\ \Omega$ is the impedance of free space. This relation is identical to the normal incidence case when graphene is immersed in a medium

TABLE I
PARAMETERS OF THE OPTIMIZED DEVICE

Parameter	Value	
	TE	TM
Effective index, n_{eff}	1.44625	1.44612
Group velocity ($\times 10^8$ m/s)	2.04117	2.04147
Chromatic Dispersion (ps/nm/km)	17	18
Insertion loss, $1 - (\mathcal{C}_{AB}\mathcal{C}_{BC})^2$ (dB)	2.2	1.6
Absorption coefficient, α_g (dB/cm)	54	0.1
Effective graphene width, w_{eff} (μm)	8.5	7.5
I_{eff} for $P_0 = 1$ kW (MW/cm^2)	710	1.8

with refractive index n_{eff}, where the absorptance is $I_g/I_{\text{eff}} = 4\eta_0\sigma' n_{\text{eff}}|2n_{\text{eff}} + \eta_0\sigma|^{-2} \approx \eta_0\sigma'/n_{\text{eff}}$. Accordingly, we define an effective interacting intensity as

$$I_{\text{eff}} = \frac{n_{\text{eff}}}{2\eta_0 w_{\text{eff}}} \int_g |\mathbf{E}_{\|}(x, y_g)|^2 dx. \tag{6}$$

The saturation parameter $s \equiv I_{\text{eff}}/I_s$, where I_s is the saturation intensity measured at normal incidence, is now directly comparable to those quoted in most works. From the device point of view, it is helpful to relate the saturation parameter to the input power P_0. We thus write $s = P_0/P_s$, where the saturation power

$$P_s = \frac{\sigma'\eta_0 w_{\text{eff}}}{n_{\text{eff}}\alpha_0\mathcal{C}_{AB}\mathcal{C}_{BC}} I_s. \tag{7}$$

Table I shows some parameters that are often used to characterize optical devices. The values are given for the optimized device ($d = 0$, $t = 0.8\ \mu$m) and monolayer undoped graphene for $\lambda = 1550$ nm.

The literature reports a wide range of values for I_s. For the lowest value of $I_s = 0.5$ MW/cm^2 [26], and for the parameters in Table I, we have that $P_{s,\text{TE}} = 0.7$ W and $P_{s,\text{TM}} = 0.3$ kW. Thus, for $P_0 = 1$ kW, the saturation parameters are $s_{\text{TE}} = 1.4 \times 10^3$ and $s_{\text{TM}} = 3.6$, and both modes experience saturation. On the other extreme, I_s of order of 1 GW/cm^2 has also been reported [27]. In such case, $P_{s,\text{TE}} = 1.4$ kW, $P_{s,\text{TM}} = 0.6$ MW, thus $s_{\text{TE}} = 0.7$ and $s_{\text{TM}} \approx 0$, and the saturation is negligible for the TM mode. The input power chosen in this example, $P_0 = 1$ kW, is of the order of the intracavity peak power in typical soliton fiber lasers.

We solve the modes of the saturated GDF by assuming a uniform conductivity of the form $\sigma_N(s) = N\sigma/(1 + s)$. A similar expression, $\alpha_{\text{sat}} = \alpha_0/(1 + s)$, is commonly used to estimate the steady state saturated value of the absorption coefficient, but as we show below, this is not valid for multilayer graphene in waveguides.

Fig. 7(a) shows the absorption coefficient for the TE mode as a function of s. Except for the monolayer case, the curves of α_g as a function of s initially depart from the $(1 + s)^{-1}$ dependence. To better evidence this departure, we have included in Fig. 7 the cases of $N = 10$,and $N = 20$, where for moderate saturation ($s \approx 1$), α_g increases with s, exhibiting a behavior that is typical of a reverse saturable absorber. We can understand this effect by noting that, in the linear case ($s \approx 0$), the TE mode is *repelled* by the large conductivity ($N\sigma$) of the graphene plane, but, as the conductivity is reduced by the saturation effect, the mode is now allowed to *move* towards the superstrate, thus increasing

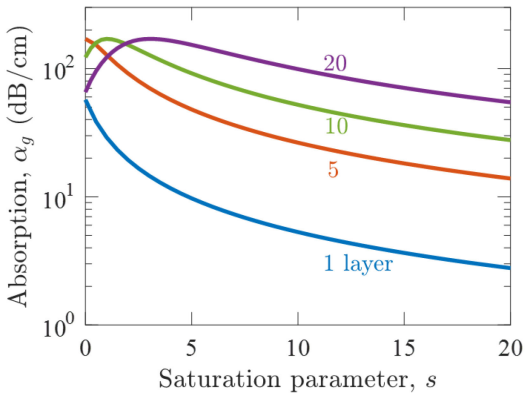

Fig. 7. Absorption coefficient as a function of the saturation parameter ($d = 0$, $t = 0.8$ μm).

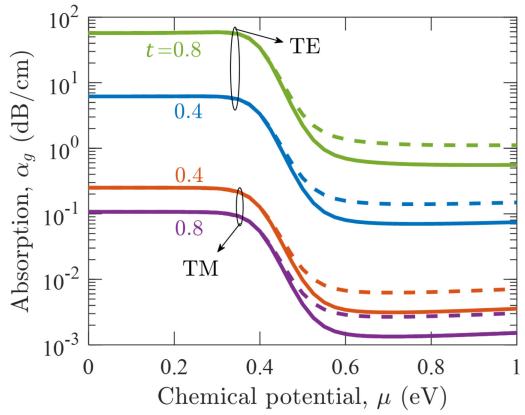

Fig. 8. Absorption loss coefficient as a function of the chemical potential. Two superstrate thicknesses are shown for each mode, solid and dashed lines are for scattering rates of 3 meV and 6 meV, respectively, and $d = 0$ in all cases.

the overlap between graphene and the mode, resulting in a larger absorption coefficient.

D. Chemical Potential and Scattering Rate

The graphene conductivity is given by [24]

$$\sigma = -\frac{ie^2}{\pi\hbar^2\Omega}\int_0^\infty E\left(\frac{\partial f(E)}{\partial E} - \frac{\partial f(-E)}{\partial E}\right)dE + \frac{ie^2\Omega}{\pi\hbar^2}\int_0^\infty \frac{f(-E)-f(E)}{\Omega^2 - 4(E/\hbar)^2}dE, \quad (8)$$

where $\Omega = 2\pi c/\lambda + i2\Gamma$, Γ is the scattering rate, $\hbar$ is the reduced Planck constant, c is the speed of light, and e is the electronic charge. $f(E) = [\exp[(E-\mu)/(k_BT)]+1]^{-1}$ is the Fermi-Dirac distribution function, where k_B is the Boltzmann constant, μ the chemical potential, and T the absolute temperature. The first (second) term on the right-hand side of (8) is due to intraband (interband) transitions.

Fig. 8 shows α_g as a function of the chemical potential (μ) for two superstrate thickness, using scattering rates of $\hbar\Gamma = 3$ meV and $\hbar\Gamma = 6$ meV, which correspond to $\tau = 110$ fs and $\tau = 55$ fs, respectively, by means of the relation $\tau = \hbar/(2\Gamma)$. For $|\mu| \geq 0.6$ eV, the interband conductivity is zero, and the absorption is due to intraband transitions.

The chemical potential can be controlled by applying an external electric field, as in the case of optical modulators or switches (we do not consider these devices, as they require an additional electrode that modifies the modes). Another cause for the variation of $|\mu|$ is unintentional doping, which is very common in graphene samples obtained by exfoliation (μ_{exf}) or by chemical vapor deposited (μ_{CVD}) and transferred to glass substrates. Refs. [28] and [29] report measurements of the unintentional doping of graphene on a SiO_2 substrate for exfoliated and CVD graphene, respectively, and for a variety of different sample qualities. Considering mean values of the doping concentrations: $p_{0,\text{exf}} = 9\times10^{12}$ cm^{-2} and $p_{0,\text{CVD}} = 4\times10^{12}$ cm^{-2} [30], we obtain $|\mu_{\text{exf}}| = 0.38$ eV, $|\mu_{\text{CVD}}| = 0.25$ eV at $T = 300$ K. We see that for the unintentional doping of CVD graphene, the results are virtually the same as those for no doping. For exfoliated graphene, on the other hand, $|\mu_{\text{exf}}|$ is close to one half of the photon energy (0.4 eV), where the absorption varies considerably. In practice, however, for a GDF device, one is more likely to use CVD graphene, because of the large area needed.

IV. Conclusion

In conclusion, when graphene is deposited on top of a waveguide, its interaction with light can be widely adjusted through the waveguide design. We have studied how the GDF with a superstrate ($n = 1.490$) depends on the geometrical parameters (d and t), graphene intrinsic parameters (chemical potential and scattering rate), number of layers, and input power. For all the space of variation of these parameters we find that the TE mode is more absorbed than the TM mode. The nonlinear optical absorption can be thoroughly characterized by the absorbed intensity, which takes into account the spatial overlap of the mode with graphene, polarization and the power coupling from the input standard fiber to the GDF.

We propose parameters that facilitate the analysis and characterization of the GDF as saturable absorber: an effective graphene width (w_{eff}), an average absorbed intensity I_g, (4), and an effective intensity w_{eff}, (6), equivalent to the intensity of a normal incident wave producing the same I_g. These parameters should be useful for the analysis of other nonlinear effects and other waveguide profiles incorporating graphene or other 2D nonlinear absorbers.

Our calculations show that a near-zero gap distance between the fiber core and graphene is advantageous, since it provides a strong graphene-light interaction without introducing a substantial coupling loss. Additionally, a superstrate layer with a refractive index slightly higher than that of the fiber core greatly improves the graphene-light interaction for the TE mode. Increasing the superstrate thickness produces a larger overlap of the TE mode with graphene that overcomes the somewhat larger coupling loss in comparison with the TM mode. However, this improvement is limited by the appearance of the second order mode for a thickness whose precise value depends on the superstrate refractive index. We find that, for a superstrate with

$n = 1.49$ (typical of polymers such as PMMA) with thickness of $0.7 - 0.8\ \mu$m, the GDF is single mode with a strong interaction. Thus, a device with $d = 0$ and $t = 0.8\ \mu$m is an optimum single mode saturable absorber device at $\lambda = 1550$ nm. This device can be fabricated using the standard fabrication methods of polished fibers and spin coating of the superstrate. Usually the thickness of the PMMA superstrate is 300 nm [11]. Nevertheless, the optimum thickness is easy to be fabricated. This GDF device operates at $\lambda \geq 1450$ nm. At shorter wavelengths, the superstrate thickness needs to be reduced in order to maintain single mode operation.

For $P_0 = 1$ kW input peak power (which is typical of intracavity soliton fiber lasers), we find that the TE mode of the optimized device reaches a saturation parameter of $s \geq 1$ for any value of $I_s \leq 730\ \mathrm{MW/cm^2}$. This optimized device also works as an excellent in-line polarizer.

We have shown that the graphene-light interaction is maximized for 5 layers. Furthermore, we predict that, by further increasing the number of layers, the GDF acts as a reverse saturable absorber. We explained this peculiar behavior as a result of the antagonism between the *repulsion* of the TE mode by the large conductivity and the *attraction* of the mode by the superstrate. When the effective intensity increases, saturation reduces the conductivity and the mode is more *attracted* to the superstrate, and thus increasing the absorption.

The same approach can be used for other waveguides and other materials. In particular, for superstrate materials with a higher refractive index, such as SU-8, the optimized single mode device uses a thinner superstrate layer. We believe that this study may help in designing optimized 2D-based waveguide devices such as polarizers, saturable absorbers, modulators, detectors, and sensors.

ACKNOWLEDGMENT

The authors would like to thank the Sao Paulo Research Foundation (FAPESP) (2019/16793-6, 2018/08988-9, 2018/25339-4) and CAPES.

REFERENCES

[1] Y.-W. Song, S.-Y. Jang, W.-S. Han, and M.-K. Bae, "Graphene mode-lockers for fiber lasers functioned with evanescent field interaction," *Appl. Phys. Lett.*, vol. 96, no. 5, 2010, Art. no. 051122.

[2] M. Jung et al., "Mode-locked pulse generation from an all-fiberized, tm-ho-codoped fiber laser incorporating a graphene oxide-deposited side-polished fiber," *Opt. Exp.*, vol. 21, pp. 20062–20072, Aug. 2013.

[3] H. Ahmad, S. Soltani, K. Thambiratnam, M. Yasin, and Z. Tiu, "Mode-locking in Er-doped fiber laser with reduced graphene oxide on a side-polished fiber as saturable absorber," *Opt. Fiber Technol.*, vol. 50, pp. 177–182, 2019.

[4] S. Y. Choi, H. Jeong, B. H. Hong, F. Rotermund, and D.-I. Yeom, "All-fiber dissipative soliton laser with 10.2 nJ pulse energy using an evanescent field interaction with graphene saturable absorber," *Laser Phys. Lett.*, vol. 11, no. 1, Nov. 2013, Art. no. 015101.

[5] A. L. Khalaf et al., "Room temperature ammonia sensor using side-polished optical fiber coated with graphene/polyaniline nanocomposite," *Opt. Mater. Exp.*, vol. 7, no. 6, pp. 1858–1870, Jun. 2017.

[6] J. Zhang et al., "All-fiber-optic temperature sensor based on reduced graphene oxide," *Laser Phys. Lett.*, vol. 11, no. 3, Feb. 2014, Art. no. 035901.

[7] N. M. Y. Zhang et al., "Hybrid graphene/gold plasmonic fiber-optic biosensor," *Adv. Mater. Technol.*, vol. 2, no. 2, 2017, Art. no. 1600185.

[8] Y. Xiao et al., "Theoretical investigation of optical modulators based on graphene-coated side- polished fiber," *Opt. Exp.*, vol. 26, no. 11, pp. 13759–13772, May 2018.

[9] P. C. Debnath, S. Uddin, and Y.-W. Song, "Ultrafast all-optical switching incorporating in situ graphene grown along an optical fiber by the evanescent field of a laser," *ACS Photon.*, vol. 5, no. 2, pp. 445–455, 2018.

[10] E. J. Lee et al., "Active control of all-fibre graphene devices with electrical gating," *Nat. Commun.*, vol. 6, no. 1, Apr. 2015, Art. no. 6851.

[11] J. D. Zapata, D. Steinberg, L. A. M. Saito, R. E. P. de Oliveira, A. M. Cárdenas, and E. A. T. de Souza, "Efficient graphene saturable absorbers on D-shaped optical fiber for ultrashort pulse generation," *Sci. Rep.*, vol. 6, no. 1, Feb. 2016, Art. no. 20644.

[12] Q. Bao et al., "Broadband graphene polarizer," *Nat. Photon.*, vol. 5, no. 7, pp. 411–415, Jul. 2011.

[13] H. Zhang et al., "Graphene-based fiber polarizer with PVB-enhanced light interaction," *IEEE J. Lightw. Technol.*, vol. 34, no. 15, pp. 3563–3567, Aug. 2016.

[14] R. Chu et al., "High extinction ratio D-shaped fiber polarizers coated by a double graphene/PMMA stack," *Opt. Exp.*, vol. 25, no. 12, pp. 13278–13285, Jun. 2017.

[15] K.-J. Peng et al., "Saturated evanescent-wave absorption of few-layer graphene-covered side-polished single-mode fiber for all-optical switching," *Nanophotonics*, vol. 7, no. 1, pp. 207–215, 2018.

[16] N. H. Park, H. Jeong, S. Y. Choi, M. H. Kim, F. Rotermund, and D.-I. Yeom, "Monolayer graphene saturable absorbers with strongly enhanced evanescent-field interaction for ultrafast fiber laser mode-locking," *Opt. Exp.*, vol. 23, no. 15, pp. 19806–19812, Jul. 2015.

[17] X. Li et al., "High-power graphene mode-locked Tm/Ho co-doped fiber laser with evanescent field interaction," *Sci. Rep.*, vol. 5, no. 1, Nov. 2015, Art. no. 16624.

[18] H. Jeong et al., "All-fiber tm-doped soliton laser oscillator with 6 nJ pulse energy based on evanescent field interaction with monoloayer graphene saturable absorber," *Opt. Exp.*, vol. 24, no. 13, pp. 14152–14158, Jun. 2016.

[19] W. Li, L. Yi, R. Zheng, Z. Ni, and W. Hu, "Fabrication and application of a graphene polarizer with strong saturable absorption," *Photon. Res.*, vol. 4, no. 2, pp. 41–44, Apr. 2016.

[20] B. C. Yao et al., "Graphene based widely-tunable and singly-polarized pulse generation with random fiber lasers," *Sci. Rep.*, vol. 5, no. 1, Dec. 2015, Art. no. 18526.

[21] H. Zhang, N. Healy, L. Shen, C. C. Huang, D. W. Hewak, and A. C. Peacock, "Enhanced all-optical modulation in a graphene-coated fibre with low insertion loss," *Sci. Rep.*, vol. 6, no. 1, Mar. 2016, Art. no. 23512.

[22] X. Liu, L. Yang, J. Ma, C. Li, W. Jin, and W. Bi, "Study on polarization properties of graphene coated D-shaped fiber," *Chin. Phys. B*, vol. 27, no. 10, Oct. 2018, Art. no. 104206.

[23] R. E. P. de Oliveira and C. J. S. de Matos, "Graphene based waveguide polarizers: In-depth physical analysis and relevant parameters," *Sci. Rep.*, vol. 5, no. 1, Nov. 2015, Art. no. 16949.

[24] G. W. Hanson, "Dyadic green's functions and guided surface waves for a surface conductivity model of graphene," *J. Appl. Phys.*, vol. 103, no. 6, 2008, Art. no. 064302.

[25] D. F. Londono-Giraldo, "Nonlinear optical devices based on graphene atop waveguides," Ph.D. dissertation, Universidade Presbiteriana Mackenzie, Sao Paulo, Brazil, Feb. 2022. [Online]. Available: https://dspace.mackenzie.br/handle/10899/28921

[26] Q. Bao et al., "Atomic-layer graphene as a saturable absorber for ultrafast pulsed lasers," *Adv. Funct. Mater.*, vol. 19, no. 19, pp. 3077–3083, 2009.

[27] A. Malouf, O. Henderson-Sapir, S. Set, S. Yamashita, and D. J. Ottaway, "Two-photon absorption and saturable absorption of mid-IR in graphene," *Appl. Phys. Lett.*, vol. 114, no. 9, 2019, Art. no. 091111.

[28] J. M. Caridad, F. Rossella, V. Bellani, M. Maicas, M. Patrini, and E. Díez, "Effects of particle contamination and substrate interaction on the raman response of unintentionally doped graphene," *J. Appl. Phys.*, vol. 108, no. 8, 2010, Art. no. 084321.

[29] T. Ciuk et al., "Properties of chemical vapor deposition graphene transferred by high-speed electrochemical delamination," *J. Phys. Chem. C*, vol. 117, no. 40, pp. 20833–20837, 2013.

[30] D. Castelló-Lurbe, H. Thienpont, and N. Vermeulen, "Predicting graphene's nonlinear-optical refractive response for propagating pulses," *Laser Photon. Rev.*, vol. 14, no. 6, 2020, Art. no. 1900402.

Daniel Felipe Londono-Giraldo received the B.Sc. degree in telecommunications engineering from the Universidad de Antioquia, Medellin, Colombia, in 2017, and the Ph.D. degree in electrical and computer engineering from Universidade Presbiteriana Mackenzie, Sao Paulo, Brazil, in 2022. During the Ph.D. degree, he was with the modeling and design of nonlinear optical devices based on graphene atop waveguides.

Eunezio Antonio Thoroh De Souza received the B.S. degree in physics from the University of São Paulo, SPaulo, Brazil, in 1986 and the Ph.D. degree in physics from the University of Campinas, Campinas, Brazil, in 1991. From 1992 to 1995, he was a Visiting Researcher with AT&T Bell Laboratories (Homdel, NJ) with the Department of Advanced Optoelectronic Devices. Back in Brazil, he became an Adjunct Professor with the Physics Institute of the University of Brasília, Brasa, Brazil, where he coordinated the graduate program of the Institute of Physics. He is currently a Full Professor of physics, E.E. and material science with Mackenzie Presbyterian University, SPaulo, Brazil, and the creator of MackGraphe (Graphene and Nanomaterials Research Center). He is an advisor to CGIA (China Innovation Alliance of the Graphene Industry), Member of the International Committee of FAPESP's Research, member of CPqD's Innovation Committee and member of Optical Society of America. His main interests include 2D materials, photonics, and ultrafast sources.

Hugo Luis Fragnito received the Licenciado degree in physics from the University of Buenos Aires, Buenos Aires, Argentina in 1976, and the Doctor of Sciences from the State University of Campinas, Campinas, Brazil, in 1984. He was a Research Visitor with the Università di Roma, Roma, Italy during 1980–1981, AT&T Bell Laboratories, Holmdel, NJ, USA during 1987–1989. In 1978, he joined Unicamp and the Mackenzie Presbyterian University, São Paulo, Brazil, during 2015–2020. His research interests include nonlinear optics and optical modulators in waveguides incorporating graphene and other 2D materials, and their applications in communications systems.